Numerical study of electronic transport in gated graphene ribbons

Alessandro Cresti,[1,2,3] Giuseppe Grosso,[1,2] and Giuseppe Pastori Parravicini[1,4]
[1]*NEST-CNR-INFM, Piazza dei Cavalieri, I-56126 Pisa, Italy*
[2]*Dipartimento di Fisica "E. Fermi," Università di Pisa, Largo Pontecorvo 3, I-56127 Pisa, Italy*
[3]*Scuola Normale Superiore, Piazza dei Cavalieri 7, I-56126 Pisa, Italy*
[4]*Dipartimento di Fisica "A. Volta," Università di Pavia, Via A. Bassi 6, I-27100 Pavia, Italy*
(Received 15 June 2007; revised manuscript received 10 September 2007; published 26 November 2007)

Electron transport and current profiles through gated graphene ribbons are addressed within the tight-binding Keldysh formalism. Conductance, conductivity, and current quantum shot noise are studied numerically as functions of the width of the ribbons, length of the gated region, and strength of the gate potential. Crossover between pseudodiffusive and ballistic transport regimes is examined in detail. In particular, around the energy of the gate potential, it is shown that the pseudodiffusive regime occurs even for moderate potential strengths, well below the onset of the sp^2 hybridized bands of graphene. These findings are supported by the evaluation of current profiles of the massless Dirac fermions throughout graphene ribbons.

DOI: 10.1103/PhysRevB.76.205433 PACS number(s): 81.05.Uw, 73.63.−b, 73.50.Td

I. INTRODUCTION

The experimental realization of monolayers of carbon atoms[1–3] has opened a new area of investigation with far reaching perspectives in fundamental and applied physics. A subsequent huge number of papers have been devoted to evidence the striking mechanical, electronic, and transport properties of monolayers and bilayers of graphene, rooted to the underlying honeycomb lattice topology (see, for instance Refs. 4–7 and references quoted therein).

The breaking novelties of the papers[1–3] can be better appreciated by considering that the theoretical study of the electronic structure of ideal two-dimensional graphene started 60 yr ago with the pioneering work of Wallace.[8] Since then, the quest for deeper understanding of the electronic structure of graphene, graphite, and carbon based compounds has never ceased, as testified by early and recent works (for instance Refs. 9–15 and references therein).

Most of the remarkable and unique properties of graphene are connected to its peculiar conical bands[16] in the low energy electronic excitation spectrum. In fact, it is accepted that the Dirac-like shape of the electronic dispersion at the corners of the graphene Brillouin zone is responsible for the observed half integer quantum Hall effect[2,3] [$G_H = \pm(4e^2/h) \times (n+1/2)$, where n is the integer Landau level index], for the minimum conductivity of graphene ribbons,[2,5] for the possibility of easy tunneling through arbitrarily high and large barriers (Klein paradox[17]), and for the role of Zitterbewegung[18,19] as intrinsic disorder effect. In particular, the comprehension of the residual conductivity of pure graphene ribbons in the limiting case of vanishing carriers and density of states is currently under debate mainly due to the "π discrepancy" between the observed values ($\sigma_{xx}^{\min} = 4e^2/h$) and the most frequently proposed theoretical values ($\sigma_{xx}^{\min} = 4e^2/\pi h$). Furthermore, the theoretical results for minimum conductivity,[18–23] which are generally obtained by means of Kubo theory, Landauer formalism, or field theory techniques, not always agree on the numeric coefficient in front of the $4e^2/h$ term. The degree of robustness of the minimum conductivity of graphene has also been discussed against several impurity scattering potentials[21–25] or electron-electron interactions.[26]

Much interest has been devoted to the transport properties of clean graphene ribbons in the presence of gated regions of width W and length L. Ideally, clean, short, and wide gated samples ($W/L \gg 1$) may behave[20] as conventional disordered metallic systems, in spite of the fact that the flow of carriers in graphene ribbons occurs in the absence of impurities, lattice defects, or other scattering mechanisms. The transport regime of wide and short strips of graphene has been dubbed as "pseudodiffusive" when the basic universal features[20] are indiscernible from the ones of classical diffusive systems. In particular, the conductance of graphene strips may exhibit Ohmic behavior (conductance $G = \sigma W/L$), while, concomitantly, the Fano factor[27] for shot noise approaches the universal value 1/3, typical of classical diffusive systems. The conditions for manifestation of pseudodiffusive transport phenomenology or ballistic behavior in gated graphene ribbons are investigated and clarified in this paper by means of accurate numerical simulations.

In Sec. II, we consider some basic aspects of the tight-binding Keldysh formalism for the numerical study of charge transport and current profiles in two-dimensional graphene ribbons. In Sec. III, conductance, conductivity, current shot noise, and current profiles are evaluated for various values of the width of the ribbon, length of the gated region, and strength of the applied gate potential. We discuss the conditions that lead to the Ohmic behavior of the system and examine the crossover between pseudodiffusive and ballistic regimes. Section IV contains the conclusions.

II. SYNOPSIS OF THE THEORETICAL AND COMPUTATIONAL BACKGROUND

In the theoretical study of nonequilibrium properties of mesoscopic systems, the Keldysh-Green function formalism has evolved into a most powerful tool for the description of quantum transport.[28–30] This is due from one side to its fully general formal foundations and from the other to its flexibility to lend itself to accurate numerical calculations of the

kinetic equations. Actually, the Keldysh formalism comprises the full many-body quantum theory. Appropriate self-energy operators $\Sigma^{R,A,<,>)(scatt)}$ (retarded, advanced, lesser, and greater), worked out by diagrammatic techniques, can, in principle, account for the presence and effects of the many-body interactions (such as electron-phonon, electron-electron, surface roughness, disorder scattering of alloys and impurities, and dephasing effects); indeed, a number of significant models of many-body interactions can be worked out at the desired, or at least reasonable, level of sophistication. Last but not the least, the self-energy operators $\Sigma^{R,A,<,>)(leads)}$ due to the open leads on the active device region are embodied exactly in the theory and computed with high accuracy by means of the renormalization-decimation or other recursive techniques.

In particular, the transport properties of two-dimensional square lattices, which simulate the conventional electron gas at the interface of GaAs-AlGaAs structures, have been investigated in a number of papers with the nonequilibrium Green's function approach,[31–36] also in the presence of magnetic fields, disorder effects, and quantum point contacts. The formulation of the Keldysh nonequilibrium Green's function theory in the framework of the tight-binding representation of the electronic system has been thoroughly studied in Ref. 32, where convenient expressions and procedures for the evaluation of space and energy resolved spectral currents are reported. In the case of one-electron Hamiltonians, the ingredients necessary to evaluate conductance, shot noise, space, and energy resolved current profiles, only involve propagators among orbitals belonging to single transverse sections of the system, arbitrarily scanned through the device.

For the study of transport of graphene nanoribbons, we have found a route from the well established procedures for square lattices to the hexagonal honeycomb topology. We do not dwell here in concepts, implementations, and details, except for the following remark. In the square lattice topology (with nearest-neighbor interactions), intracolumn matrices are tridiagonal and nearest-neighbor intercolumn matrices are diagonal.[32] Both properties also hold for the hexagonal honeycomb topology, with the difference that alternate elements of the upper and lower diagonals of intracolumn matrices are zero. Moreover, the presence of imperfections, disordered potentials in selected regions, boundary roughness, and other disruptions can be handled by properly defining site and hopping tight-binding parameters.

III. RESULTS AND DISCUSSION

In this section, we begin with a few considerations on the electronic structure of graphene and graphene ribbons of relevance in the following. We focus our attention on the π bands that originate from the dangling p_z orbitals of the two carbon atoms in the graphene primitive cell. The hopping parameter between two nearest-neighbor p_z orbitals is set to $t=-3$ eV, (Ref. 13) because this value provides a satisfactory description of the energy bands near the Dirac points in an orthogonal tight-binding model. The energy of the p_z orbitals is taken as the reference energy and set equal to zero. The lattice parameter of the two-dimensional hexagonal structure of graphene is $a=2.46$ Å.

In early studies[8–12] of the electronic states of graphene, just on the basis of group theory arguments[11,12] of the little group of $\mathbf{k}$ and regardless of the actual band structure methods adopted, it was realized that the π bands of graphene are degenerate at the corner points of the hexagonal Brillouin zone and have linear energy-wave-vector dispersion nearby (Dirac points). Within the often adopted nearest-neighbor tight-binding representation, the π bands are described by the relation

$$E(\mathbf{k}) = \mp t|F(\mathbf{k})|, \tag{1a}$$

where

$$F(\mathbf{k}) = 1 + 2\cos\frac{k_x a}{2}\exp\left(-i\frac{k_y b}{2}\right), \quad b = a\sqrt{3}, \tag{1b}$$

is the geometrical structure factor pertinent to the nearest-neighbor environment of one sublattice for the honeycomb topology.

The top valence band and bottom conduction band are degenerate at the Dirac points $\mathbf{k}=(2\pi/3a,0)$ and $\mathbf{k}'=(-2\pi/3a,0)$, characterized by the equality $F(\mathbf{k})=0$. The geometrical structure factor can be linearized near the Dirac points, where Eq. (1a) becomes

$$E(\mathbf{k}) = \mp\frac{\sqrt{3}}{2}|t|ka, \quad k = \sqrt{k_x^2 + k_y^2}, \tag{1c}$$

and the typical conical shape behavior of the energy bands is recovered. Thus, carriers near the degeneracy points of graphene behave like relativistic massless Dirac particles.

The lattice structure of graphene ribbons with zigzag modulation in the longitudinal x direction is depicted in Fig. 1(a). The average width of a ribbon with N_z zigzag carbon chains is

$$W = \frac{b}{2}(N_z - 1), \quad b = a\sqrt{3} = 4.26 \text{ Å}. \tag{2}$$

A typical width $W=100$ nm corresponds to $N_z=470$. This value is the rank of the matrices handled in the implementation of the tight-binding Keldysh formalism for the simulation of charge transport. Figure 1(a) also indicates the N_z zigzag chains forming the ribbon and the $2N_z$ sites in the primitive cell of the one-dimensional wire.

The energy bands of graphene ribbons are obtained considering standard Bloch sums for each of the $2N_z$ basis atomic orbitals and diagonalizing the crystal Hamiltonian. The band structure of graphene ribbons with $N_z=470$ is reported in Figs. 1(b)–1(d) with an increasing degree of detail. In Fig. 1(b), all the bands are reported in the whole Brillouin zone, with k_x extending from $[-\pi/a, +\pi/a]$. The $2N_z$ bands are delimited by the curves $E(k_x)=\mp t\mp 2t\cos(k_x a/2)$. The flat part of the bands at $E=0$ corresponds to states completely localized at the edges of the ribbon for $k_x=\pi/a$ and penetrating into the bulk as k_x approaches the Dirac points $k_x=\pm 2\pi/3a$. In Fig. 1(c), we enlarge the energy axis and report a limited number of electron and hole energy bands around the reference energy $E=0$. From this figure, for $E>0$, it is apparent that the ground electronic band, opening at zero energy, does not share the twofold valley degeneracy of

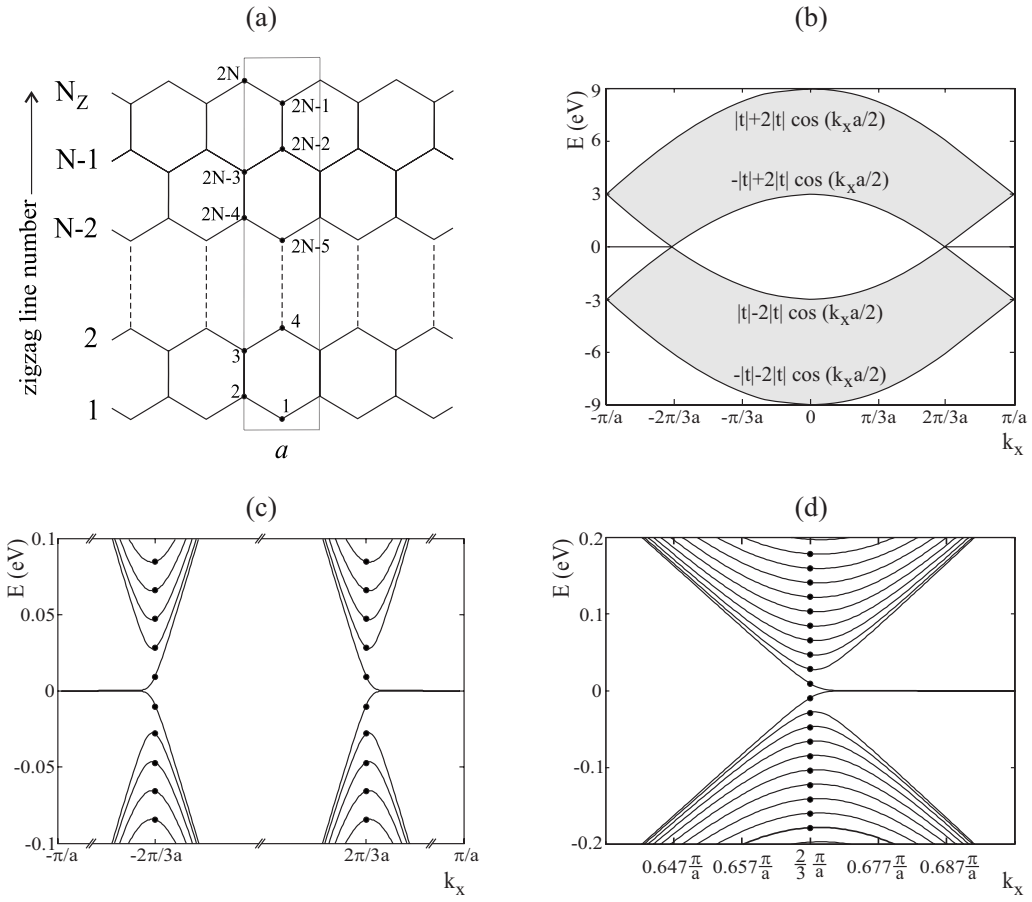

FIG. 1. (a) Lattice structure of graphene ribbons with N_z longitudinal zigzag chains along the x direction and $2N_z$ carbon atoms in the unit cell. (b) Description of all the allowed energy bands of a graphene ribbon made up of $N_z=470$ zigzag chains and width $W=100$ nm; the $2N_z$ (almost continuous) energy bands lie within the four delimiting curves $E(k_x)=\mp t\mp 2t\cos(k_x a/2)$. The surface states are also indicated. (c) Allowed energy bands of (b) near the $E=0$ reference energy. (d) Allowed energy bands of (b) around the reference energy and around one of the Dirac points. For convenience, in (c) and (d), we indicate with dots the values of the energies at the Dirac points, given by the analytic expression $E_n=\pm(n+1/2)\hbar v_F\pi/W$ of the text.

all the successive electronic bands at higher energies. For $E<0$, similar considerations can be done by virtue of the electron-hole particle symmetry. In Fig. 1(d), we show the energy bands in a small region of the Brillouin zone around the Dirac point $k_x=2\pi/3a$; it is apparent that the one-dimensional energy bands of graphene ribbons are reminiscent of the typical conical intersection of two-dimensional graphene and break into discretized electron and hole minibands due to the finite transverse dimension of the ribbon.

At the points $k_x=\pm 2\pi/3a$ of the ribbon Brillouin zone, the energies of the zigzag ribbons are given (with good approximation) by the relation[20]

$$E_n=\pm\left(n+\frac{1}{2}\right)\hbar v_F\frac{\pi}{W},\quad n=0,1,2,3,\ldots, \tag{3}$$

where $v_F=(b/2)|t|/\hbar$ is the Fermi velocity of the massless Dirac fermions at the degeneracy points of the π bands of graphene. The plus and minus signs refer to electron and hole states, respectively. We have verified that relation (3) is also supported analytically from the properties of the tridiagonal matrix Hamiltonian describing the ribbon at the Dirac points. Exploiting relation (2), Eq. (3) can be recast in the form

$$E_n=\pm\left(n+\frac{1}{2}\right)\frac{b}{2}|t|\frac{\pi}{W}=\pm\left(n+\frac{1}{2}\right)|t|\frac{\pi}{N_z-1}.$$

For a typical value of $W=100$ nm, the distance between adjacent energies E_n is

$$\Delta E=\frac{b}{2}|t|\frac{\pi}{W}\approx 20\ \text{meV}. \tag{4}$$

Thus, for positive Fermi energies up to $(3/2)\Delta E$, only one-electron conductive channel is active, and for each increase of energy ΔE, an additional conductive channel opens at both valleys. Similar behavior occurs for hole conductive channels at negative energies.

We consider now transport properties of a zigzag graphene quantum wire infinitely extended along the x direction and of width W in the y direction. A gate voltage is superimposed to the wire in a region of length L, as shown schematically in Fig. 2. The complete quantum wire structure is conceptually partitioned into two semi-infinite parts and a

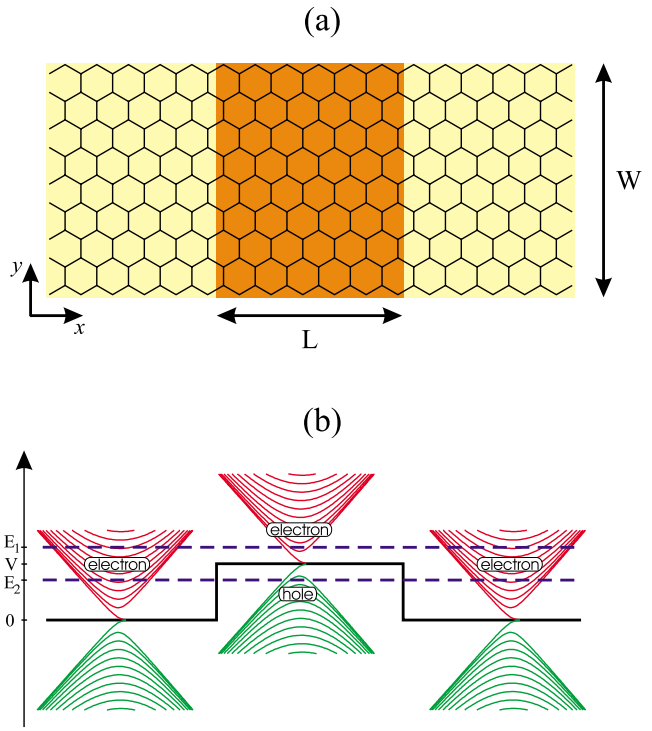

FIG. 2. (Color online) (a) Schematic representation of a zigzag graphene ribbon of width W with a superimposed top gate of length L. The effect of the gate is modeled by assigning to the sites of the gated region a constant potential of strength V. (b) Variation of the electrostatic energy potential across the ribbons. For the sake of qualitative speculations, in the left and right leads, we have reported the conical shaped energy bands of Fig. 1(d); in the central device, the same structure is reported shifted by V. The dashed lines at E_1 and E_2 denote two possible choices of the Fermi level, with electron-hole symmetry with respect to V in the gated region.

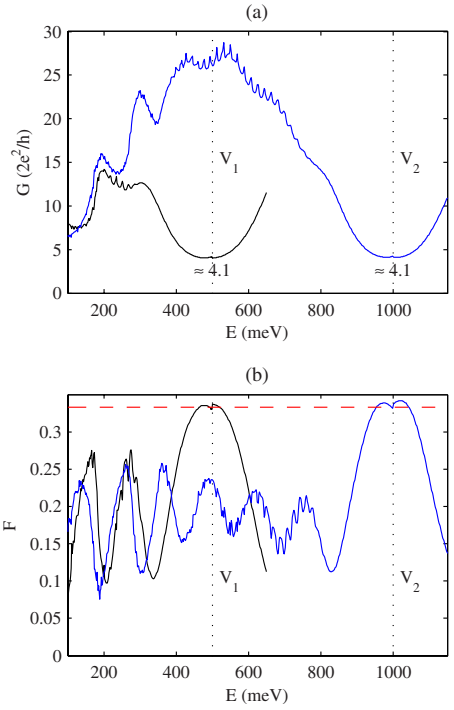

FIG. 3. (Color online) (a) Differential conductance $G(E)$ of gated graphene ribbons with $W \approx 100$ nm, $L=15$ nm, $V_1=0.5$ eV, and $V_2=1$ eV. The two curves look quite similar in an energy range around V_1 and V_2, respectively. (b) Fano factor $F(E)$ for the same graphene ribbons specified above. The shapes of the two Fano curves look quite similar for energies around V_1 and V_2, respectively, where they approach the value $F \approx 1/3$ (dotted line).

central region. The semi-infinite regions to the left and to the right of the central region behave as leads in contact with electron reservoirs at μ_L and μ_R chemical potentials. The effect of a top gate is modeled by adding a constant potential to the sites of the gated region of length L (a slightly smoothed "adiabatic" application of the gate potential is at times preferable). We begin our simulations by fixing width W and length L of the ribbon and by considering two values of the gate potential.

Figure 3(a) reports the differential conductance $G(E)$ versus Fermi energy for systems with transverse width $W=100$ nm, length $L=15$ nm, and gate potentials $V_1=0.5$ eV and $V_2=1$ eV. For E around the barrier heights V_1 and V_2, $G(E)$ exhibits the minimum value $G_{\min} \approx 4.1 \times 2e^2/h$ at the bottom of a broad valley [see Fig. 3(a)]. For energies sufficiently far from the minima, oscillations of $G(E)$ appear with period of the order of 20 meV, due to the activation or closing of successive conductive channels, in agreement with the estimated value of ΔE in Eq. (4). From the minimum value of the conductance $G_{\min} \approx 4.1 \times 2e^2/h$, we infer for the minimum conductivity $\sigma_{\min} \equiv G_{\min} L/W \approx 0.62 \times 2e^2/h$, a value very close to $\sigma_{\min}=2/\pi \times 2e^2/h$. The present numerical calculations suggest a minimal longitudinal conductivity equal to $2/\pi$ (in units of $2e^2/h$). This agrees with the currently accepted value of the minimal conductivity of an ideal honeycomb lattice. A detailed summary of approaches and corresponding numerical factors (in front of $2e^2/h$) for the minimal conductivity, provided in the literature by analytic or semianalytic methods, is given in Ref. 19. The main message of Fig. 3(a) is that the pseudodiffusive regime occurs for energies around the gate potential.

Another significant quantity for the study of transport properties is the Fano factor, i.e., the ratio between the shot noise and the Poisson noise, which is proportional to the current itself. The Fano factor can be expressed in terms of the transmission coefficient of the conductance eigenchannels T_i as

$$F = \frac{\sum_i T_i(1-T_i)}{\sum_i T_i}. \tag{5}$$

Figure 3(b) reports the Fano factors of gated graphene ribbons as a function of the Fermi energy. The two curves show broad maxima, with similar shapes around V_1 and V_2. The maxima of the Fano factor curves are about 0.32, a value very close to the universal value $1/3$ that characterizes the diffusive regime of disordered metals.

A closer inspection of Figs. 3(a) and 3(b) shows that the differential conductance $G(E)$ and the Fano factor $F(E)$ ex-

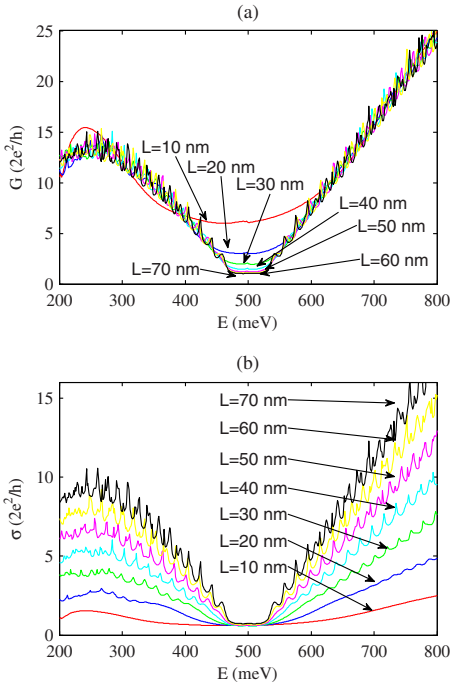

FIG. 4. (Color online) (a) Differential conductance $G(E)$ of a graphene ribbon of width $W \approx 100$ nm, gate potential $V=0.5$ eV, and several values of the gate length L (10, 20, 30, 40, 50, 60, and 70 nm from top to bottom). The curves are diffusivelike for energies near V and ballisticlike for energies far from V. (b) Conductivity $\sigma(E)=G(E)L/W$ for the same values of the gate length. For energies around V, the curves nearly overlap at the universal value $2/\pi \times 2e^2/h$ at least for small L/W.

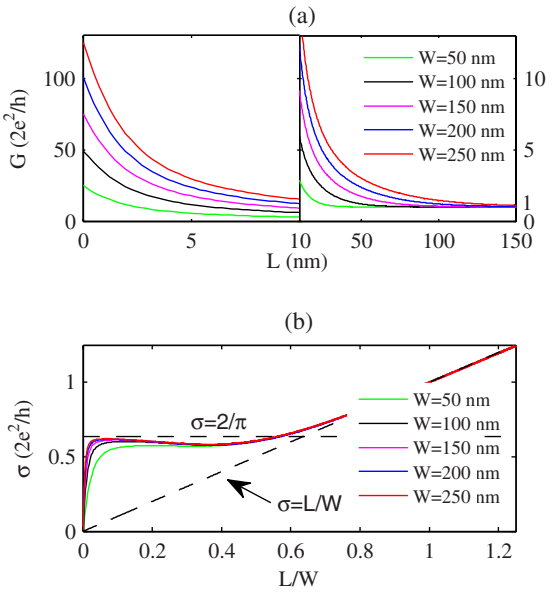

FIG. 5. (Color online) (a) Conductance of graphene ribbons as a function of L. The gate potential is $V=0.5$ eV, the Fermi energy is $E=0.505$ eV, and the ribbon widths are $W=50$, 100, 150, 200, and 250 nm (higher curves of G correspond to increasing values of W). (b) Conductivity $\sigma(E)=G(E)L/W$ for the same samples. The horizontal dotted line corresponds to $\sigma=2/\pi$ (in units $2e^2/h$); the other dotted line corresponds to $\sigma=L/W$ (in units $2e^2/h$). (In the small parameter region $L/W \ll 0.05$, higher curves of σ correspond to increasing values of W).

hibit two kinds of oscillations as a function of energy: smaller period oscillations (observed period ≈ 20 meV) and larger period oscillations (observed period ≈ 130 meV). The sample under investigation in Figs. 3 has width $W=1000$ Å and length of the gated region $L=150$ Å. From the linear energy dispersion of Eq. (1c) considering integer multiple of wave numbers π/W or π/L, we estimate the energy periods,

$$\Delta E = \frac{\sqrt{3}}{2}|t|\frac{\pi}{W}a \approx 20 \text{ meV} \quad \text{for } W = 1000 \text{ Å},$$

$$\Delta E = \frac{\sqrt{3}}{2}|t|\frac{\pi}{L}a \approx 133 \text{ meV} \quad \text{for } L = 150 \text{ Å}.$$

The close agreement between the above estimated and observed values suggests that large period oscillations are related to back-and-forth scattering of electrons in the gated region, while small period oscillations are related to the opening or closing of the successive channels, as already noted.

In Fig. 4(a), we plot the conductance $G(E)$ of graphene wires as a function of the Fermi energy for fixed width $W \approx 100$ nm, for fixed applied voltage $V=0.5$ eV, and for several values of L ($\lesssim W$). Near the energy of the Dirac points in the gated region, the conductance is approximately inversely proportional to L and independent of the energy. This occurs in an energy range of about ±30 meV around V, which is the region with just one active channel in the gated region. Far from the Dirac point at V, the conductance is approximately independent of L and varies linearly with energy (with oscillations due to the opening of new conductive channels). This behavior is indicative of an Ohmic-like transport regime around the Dirac points and of a ballisticlike regime far from them. Thus, two transport regimes may occur in the same device depending on the energy region of interest. To further highlight this issue, in Fig. 4(b), we report the quantity $\sigma(E)=G(E)L/W$. For different lengths of the gated region, the curves of $\sigma(E)$ almost collapse into the value $2/\pi \approx 0.6366$ around the Dirac energy at V while spread into a fan with (almost) linear behavior far from it.

In Fig. 5(a), we show the ribbon conductance versus length L of gated region for various widths W at fixed gate potential $V=0.5$ eV and fixed energy $E=0.505$ eV (slightly above the Dirac point energy). For convenience, a change of scale has been performed for L larger than 10 nm. The values of the conductance in the limit $L \to 0$ provide the number of open conductive channels intersected by the Fermi energy. For large L, all the conductance curves collapse into the value of $2e^2/h$. The results are better interpreted by considering the behavior of the quantity $\sigma(E)=G(E)L/W$ versus L/W, as shown in Fig. 5(b). In general, $G(E)$ and $\sigma(E)$ depend on L and W separately and not only on the quotient L/W; however, the curves of the conductivity of Fig. 5(b) present essentially three regions. For small values of L/W, the conductivity is linear in L/W, indicating a quasiballistic

behavior. For values $0.1 < L/W \lesssim 0.5$, the curves tend to a plateau of value $2/\pi$ (for large values of W). Finally, for $L/W > 1$, the system is ballistic with just one active conductive channel.

For small values of L/W and large values of W, the conductance reported in Fig. 5(a) can be approximately reproduced by the expression

$$G = \frac{2}{\pi}\frac{W}{L+L_0}\frac{2e^2}{h}, \tag{6}$$

with $L_0 \approx 13$ Å, which corresponds to the width of about ten columns of carbon atoms. The value L_0 can be regarded as a kind of dephasing length needed to reach the Ohmic regime in the gated graphene, at least for wide strips $W > L$. It is worthwhile to note that in the case of dephasing processes, site-energy fluctuations are at the origin of the Ohmic behavior. In the case of ideal graphene ribbons, when transport is mostly determined by stochastic electron transmission via evanescent modes,[20] the Ohmic regime occurs in spite of the absence of site-energy fluctuations in clean gated samples.

Expression (6), used above for fitting purpose, has been inspired by the Datta[37] model, originally developed for classical diffusive systems. According to this model, the conductance of an array of phase-incoherent scatterers in the diffusive regime (phase-relaxation length shorter than the distance between successive scatterers) is shown to take the form $G = \sigma W/(L+L_0)$, where σ is a material parameter independent of the sample dimensions, W and L are the width and the length of the two-dimensional sample, and L_0 is a characteristic length of the order of a mean free path. In spite of its simplicity (and unavoidable oversimplifications), the empirical model of Datta has some interest for heuristic considerations because it contains a minimal number of parameters (two parameters, σ and L_0, with reasonable intuitive meaning) and because the resistance of the array under attention increases linearly with the length of the array, in perfect accordance with Ohm's law.

In graphene ribbons, in the pseudodiffusive regime, the lead-to-lead transport of carriers occurs mainly via evanescent states. Regardless the peculiar microscopic mechanism of transport, it is seen that the proposed single-parameter Datta-like model of Eq. (6), with only one adjustable parameter L_0 [since σ has been fixed at the minimal conductivity value $\sigma_{\min} = 2/\pi(2e^2/h)$], can phenomenologically describe the conductance of the graphene ribbons, at least in some appropriate energy regions and geometrical shapes.

We report in Fig. 6 the Fano factors of graphene ribbons for different L, with $W \approx 200$ nm, $V = 0.5$ eV, and Fermi energy $E = 0.501$ eV. The Fano factor is almost equal to the value $1/3$ over a wide range of L ($0.05 \lesssim L/W \lesssim 0.3$). The Fano factor passes from total quenching of the shot noise for small L to the sub-Poissonian noise $F \approx 1/3$, and it remains almost equal to $1/3$ over a wide range of values of L, as far as the conductivity of Fig. 5(b) equals $2/\pi$. Finally, for increasing L, the quenching of the shot noise is recovered. We have further elaborated this last aspect of Fig. 6 by examining the transmission coefficients T_i of the eigenchannels. For all the L and W values reported in Fig. 6, and in Fig. 5, we

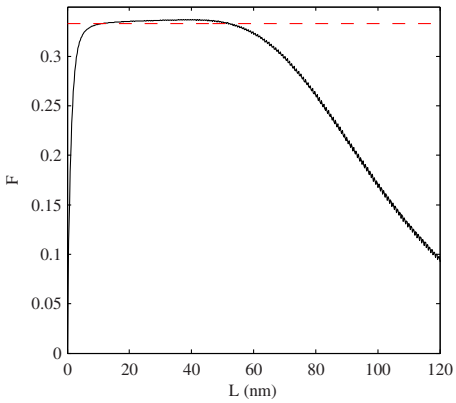

FIG. 6. (Color online) Fano factor (solid line) for a ribbon with $W \approx 200$ nm, $V = 0.5$ eV, and $E = 0.501$ eV as a function of L; the curve remains around $1/3$ (dotted line) in the range of $0.05 \lesssim L/W \lesssim 0.3$.

have observed the emergence of an eigenchannel with transmission coefficient $T \approx 1$, which is responsible for the behavior $G \approx 2e^2/h$ and $\sigma = (L/W)2e^2/h$ for large L of Fig. 5, and of the noiseless asymptotic behavior ($F \to 0$ in Fig. 6), as evident from Eq. (5). In the literature,[38] "noiseless scattering states" have been observed originally in the numerical study of electronic transport in quantum billiards; it is believed that the quantum-to-classical crossover scenarios for transport in quantum billiards are signaled by the emergence of noiseless scattering states. The noiseless scattering state, observed in graphene ribbons (with smoothed, i.e., adiabatically superimposed potential), seems to play a similar role in signaling the crossover from the pseudodiffusive to the ballistic regime.

Finally, we report in Fig. 7 some numerical results for current distributions of massless Dirac fermions. We consider a sample with $V = 0.5$ eV, $E = 0.505$ eV, and $W \approx 100$ nm and smoothed gate potentials superimposed to regions of lengths $L = 0$, 10, 50, and 100 nm. For $L = 0$, i.e., in the absence of the gate, the system and the current distribution are translationally invariant in the longitudinal direction. Many channels are active and the current is almost constant in the central part of the wire and approaches zero with oscillations at the wire edges. For $L = 10$ nm, the current in the leads flows mainly in the bulk of the wire, with several oscillations in the transverse direction near the gated region, while it is distributed almost uniformly in the gated region. Notice that the current is supported by open conductive channels in the leads and by evanescent modes in the gated region for small values of L/W. The connection between the two kinds of flows is made evident by increasing L: the transport current tends to flow only in the central part of the ribbon in the leads, while it remains almost uniform in the gated region, where transmission occurs through a decreasing number of evanescent states with unstructured contribution to the current profiles.

IV. CONCLUSIONS

We have presented a numerical study of electronic transport and current profiles in gated graphene ribbons. For en-

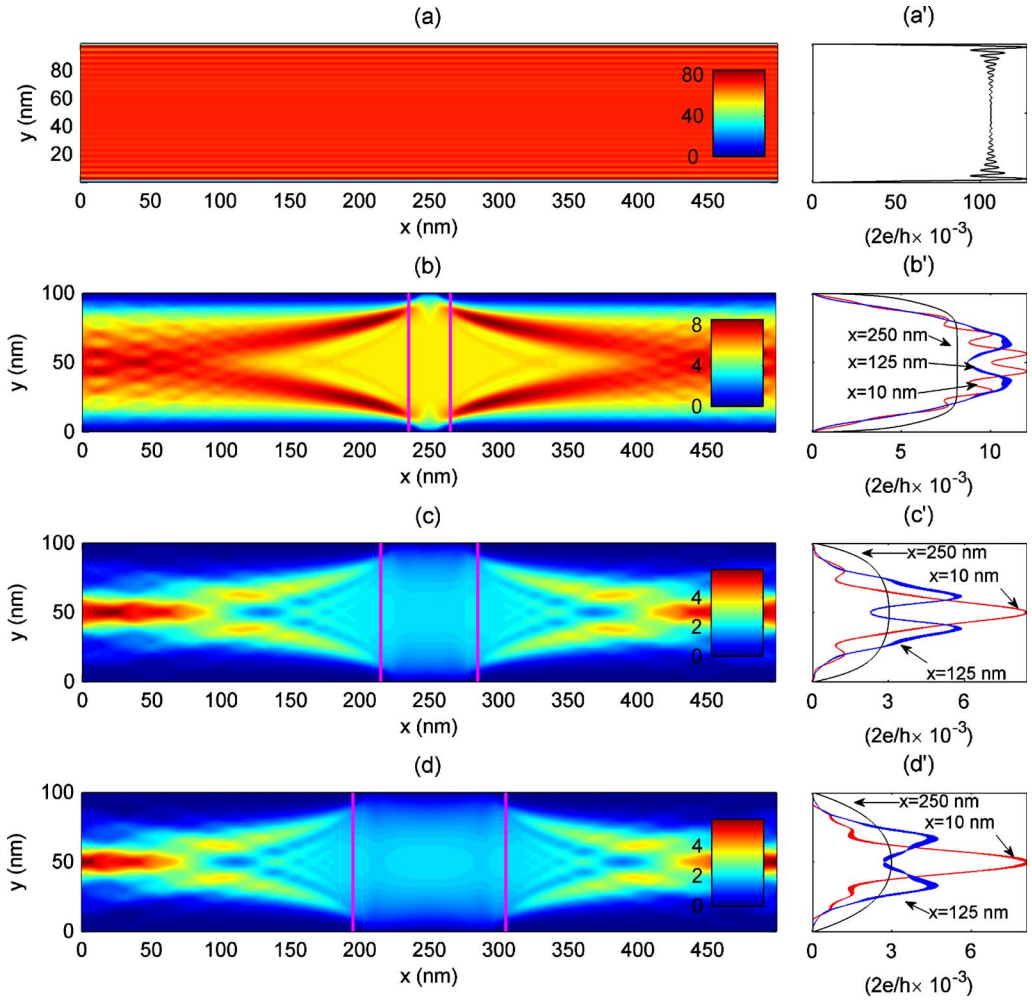

FIG. 7. (Color online) Map of the local current distribution for a graphene ribbon of width $W \approx 100$ nm, gate voltage $V=0.5$ eV, Fermi energy $E=0.505$ eV, and lengths of the gated regions $L=0$, $L=10$ nm, $L=50$ nm, and $L=100$ nm [(a), (b), (c), and (d), respectively]. The edges of the gated region are indicated by two vertical lines. In the right panels, profiles of the microscopic spectral currents along transverse sections are reported for sections at $x=250$ nm in the middle of the gated region, at $x=125$ nm in the left lead, and at $x=10$ nm, far from the gated region. The conductance in the four cases is $G=49, 3.4380, 1.1135, 1.0045 \times 2e^2/h$, respectively. The unit of the spectral current in the color scale is $i_0=(2e/h)\times 10^{-3}$.

ergies near the top of the potential barrier, with a single conductive channel active in the gated region, pseudodiffusive regime occurs. By means of a comparative study of conductivity, shot noise, and current profiles, we have examined and interpreted the crossover of pseudodiffusive transport regime and ballistic transport regime as functions of the geometrical parameters of the ribbons, of the gate potential, and of the Fermi energy. The numerical procedures adopted in this paper for graphene monolayers are suitable for generalization to other similar topological structures and should find applications in the active field of research concerning carbon materials (e.g., bilayers and nanotubes) and isoelectronic compounds (e.g., boron nitride nanostructures).

ACKNOWLEDGMENTS

This work has been supported by Scuola Normale Superiore and by National Enterprise for Nanoscience and Nanotechnology (NEST).

[1] K. S. Novoselov, A. K. Geim, S. M. Morozov, D. Jiang, Y. Zhang, S. V. Dubonos, I. V. Grigorieva, and A. A. Firsov, Science **306**, 666 (2004).

[2] K. S. Novoselov, A. K. Geim, S. V. Morozov, D. Jiang, M. I. Kastnelson, I. V. Grigorieva, S. V. Dubonos, and A. A. Firsov, Nature (London) **438**, 197 (2005).

[3] Y. Zhang, Y.-W. Tan, H. L. Stormer, and P. Kim, Nature (London) **438**, 201 (2005).

[4] C. Berger, Z. Song, X. Li, X. Wu, N. Brown, C. Naud, D. Mayou, T. Li, J. Hass, A. N. Marchenkov, E. H. Corrad, P. N. First, and W. A. de Heer, Science **312**, 1191 (2006).
[5] A. K. Geim and K. S. Novoselov, Nat. Mater. **6**, 183 (2007).
[6] J. B. Pendry, Science **315**, 1226 (2007).
[7] V. V. Cheianov, V. Fal'ko, and B. L. Altshuler, Science **315**, 1252 (2007).
[8] P. R. Wallace, Phys. Rev. **71**, 622 (1947).
[9] C. A. Coulson and H. Taylor, Proc. Phys. Soc., London, Sect. A **65**, 815 (1952).
[10] G. Dresselhaus and M. S. Dresselhaus, Phys. Rev. **140**, A401 (1965).
[11] F. Bassani and G. Pastori Parravicini, Nuovo Cimento B **50**, 95 (1967).
[12] E. Doni and G. Pastori Parravicini, Nuovo Cimento B **64**, 117 (1969).
[13] R. Saito, G. Dresselhaus, and M. S. Dresselhaus, *Physical Properties of Carbon Nanotubes* (Imperial, London, 1998).
[14] G. Grosso and G. Pastori Parravicini, *Solid State Physics* (Academic, London, 2000).
[15] B. Partoens and F. M. Peeters, Phys. Rev. B **74**, 075404 (2006).
[16] G. W. Semenoff, Phys. Rev. Lett. **53**, 2449 (1984).
[17] M. I. Kastnelson, K. S. Novoselov, and A. K. Geim, Nat. Phys. **2**, 620 (2006).
[18] M. I. Kastnelson, Eur. Phys. J. B **51**, 157 (2006).
[19] J. Cserti, Phys. Rev. B **75**, 033405 (2007).
[20] J. Tworzydlo, B. Trauzettel, M. Titov, A. Rycerz, and C. W. J. Beenakker, Phys. Rev. Lett. **96**, 246802 (2006).
[21] K. Nomura and A. H. MacDonald, Phys. Rev. Lett. **98**, 076602 (2007).
[22] K. Ziegler, Phys. Rev. Lett. **97**, 266802 (2006).
[23] N. M. R. Peres, A. H. Castro Neto, and F. Guinea, Phys. Rev. B **73**, 195411 (2006).
[24] N. M. R. Peres, F. Guinea, and A. H. Castro Neto, Phys. Rev. B **73**, 125411 (2006).
[25] E. Louis, J. A. Vergés, F. Guinea, and G. Chiappe, Phys. Rev. B **75**, 085440 (2007).
[26] E. G. Mishchenko, Phys. Rev. Lett. **98**, 216801 (2007).
[27] C. W. J. Beenakker and M. Büttiker, Phys. Rev. B **46**, 1889 (1992).
[28] D. K. Ferry and S. M. Goodnick, *Transport in Nanostructures* (Cambridge University Press, Cambridge, 1997).
[29] R. Lake, G. Klimeck, R. C. Bowen, and D. Jovanovich, J. Appl. Phys. **81**, 7845 (1997).
[30] S. Datta, *Quantum Transport: Atom to Transistor* (Cambridge University Press, Cambridge, 2005).
[31] A. Cresti, R. Farchioni, G. Grosso, and G. P. Parravicini, Phys. Rev. B **68**, 075306 (2003).
[32] A. Cresti, G. Grosso, and G. Pastori Parravicini, Eur. Phys. J. B **53**, 537 (2006).
[33] M. Mendoza and P. A. Schulz, Phys. Rev. B **71**, 245303 (2005).
[34] G. Metalidis and P. Bruno, Phys. Rev. B **72**, 235304 (2005).
[35] F. Triozon and S. Roche, Eur. Phys. J. B **46**, 427 (2005).
[36] A. Cresti, J. Appl. Phys. **100**, 053711 (2006); Nanotechnology **18**, 055403 (2007).
[37] S. Datta, *Electronic Transport in Mesoscopic Systems* (Cambridge University Press, Cambridge, 1995), p. 197.
[38] S. Rotter, F. Aigner, and J. Burgdörfer, Phys. Rev. B **75**, 125312 (2007), and reference therein.